JOURNAL OF GEOPHYSICAL RESEARCH, VOL. 98, NO. A12, PAGES 21,571–21,580, DECEMBER 1, 1993

# Interference Patterns in the Spacelab 2 Plasma Wave Data: Lower Hybrid Waves Driven by Pickup Ions

WEI FENG, DONALD A. GURNETT, AND IVER H. CAIRNS

*Department of Physics and Astronomy, University of Iowa, Iowa City*

During the Spacelab 2 mission the University of Iowa's Plasma Diagnostics Package (PDP) was released from the shuttle to explore the plasma environment around the shuttle. Wideband spectrograms were obtained from the PDP at frequencies from 0 to 30 kHz and distances up to 400 m from the shuttle. The wideband data frequently showed antenna interference patterns when the PDP was on the downstream side of the shuttle. Analysis of these interference patterns allows a determination of the wavelength, the plasma rest frame frequency, the direction of propagation, the power spectrum, and in some cases the location of the source. We concentrate our analysis on interference patterns due to lower hybrid waves: waves which have rest frame frequencies near the lower hybrid frequency and propagate perpendicular to the magnetic field. The waves have an almost flat dispersion relation with frequencies just above the lower hybrid frequency and relatively short wavelengths (1–4 m). The observed lower hybrid waves depend strongly on the position of the PDP relative to the shuttle and the magnetic field direction. Our results confirm previous suggestions that the lower hybrid waves are generated primarily in the vicinity of the shuttle and that they are driven by a charge exchange interaction between the ambient ionosphere and a $H_2O$ cloud around the shuttle.

## 1. INTRODUCTION

This paper focuses on the lower hybrid waves observed by the Plasma Diagnostics Package (PDP) spacecraft during the Spacelab 2 mission. This mission, launched on July 29, 1985, had a nearly circular, low-inclination orbit with an altitude of ~320 km and an inclination of 49.5°. A small free-flying spacecraft, the Plasma Diagnostics Package (PDP), was released from the shuttle to explore the plasma environment around the shuttle. During the 6-hour free-flight phase of the mission, the PDP completed two fly-arounds of the shuttle at distances up to 400 m. In addition to the fly-arounds a series of wake transits were preformed to survey the wake region directly downstream from the shuttle. The PDP spacecraft carried a full complement of particle and field instruments. Reviews of the instruments, the PDP spacecraft, and the observations are given by *Shawhan* [1982] and *Kurth and Frank* [1990].

Intense plasma wave turbulence has been observed by the PDP plasma wave receiver and Langmuir probe during the Spacelab 2 flight [*Gurnett et al.*, 1988; *Pickett et al.*, 1989; *Cairns and Gurnett*, 1991*a*, *b*]. The highest intensities occurred downstream from the shuttle and along magnetic field lines passing near the shuttle. The intensities also tend to increase during times of frequent thruster firings. *Paterson and Frank* [1989] show that the shuttle is surrounded by an energized distribution of $H_2O^+$ ions which is believed to be produced by a charge exchange interaction between a water cloud outgassed from the shuttle and ambient ionospheric $O^+$ ions. *Cairns and Gurnett* [1991*a*] point out that the amplitude and spectral character of the plasma waves observed by the PDP is controlled by the angle between the magnetic field and the velocity vector of the shuttle relative to the ionospheric plasma. Large wave amplitudes and a characteristic "mushroom-shaped" frequency-time structure (Figure 1, reproduced from Figure 1 of *Cairns and Gurnett* [1991*a*]) are observed in the broadband electric field spectrum when the shuttle velocity vector is nearly perpendicular to the magnetic field. The top of the mushroom consists of waves at the lower hybrid frequency. The base of the mushroom is a triangular-shaped emission which starts at low frequencies and extends up to the lower hybrid frequency near the center of the mushroom. As will be shown later, the wideband waves presented in this paper are associated with the top of the mushroom features. *Cairns and Gurnett* [1991*a*] interpreted the base of the mushroom as Doppler-shifted lower hybrid waves driven by water ions produced via a charge exchange process. They suggested that the waves are generated both locally and in the vicinity of the shuttle. The shuttle-associated waves observed in the near zone have been characterized and interpreted in detail by *Cairns and Gurnett* [1991*b*]. The near zone is defined as the region within 10 m of the shuttle. Waves from near-zero frequency to the lower hybrid frequency are interpreted as Doppler-shifted lower hybrid waves driven by beam-arc distributions [*Cairns*, 1990] of water ions formed in the vicinity of the shuttle. On the basis of these ideas, *Rivas and Hastings* [1992] have done further work on the near zone waves. They interpreted the top and bottom regions of the mushroom as lower hybrid waves propagating in different directions.

The results presented here are from the PDP plasma wave instrument which was comprised of the wideband receiver, the medium-frequency receiver (MFR), the IMP receiver, and the Helios receiver. We will focus on interference patterns observed in the wideband data. Wideband spectrograms were obtained from the PDP at frequencies from 0 to 30 kHz and at distances up to 400 m from the shuttle. Antenna interference patterns were frequently observed in the wideband data when the PDP was downstream from the shuttle. Two classes of interference patterns were observed: type 1, corresponding to waves that were associated with the ejection of an electron beam from the shuttle; and type 2, corresponding to lower hybrid waves driven by charge exchange ions. The lower hybrid waves have frequencies in



Paper number 93JA01851.
0148-0227/93/93JA-01851$05.00

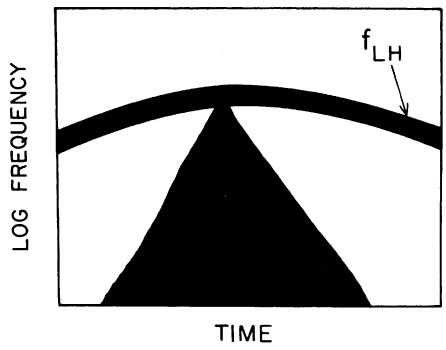


Fig. 1. An idealized "mushroom" spectral feature copied from *Cairns and Gurnett* [1991]. This spectrum is plotted on a semilog scale.

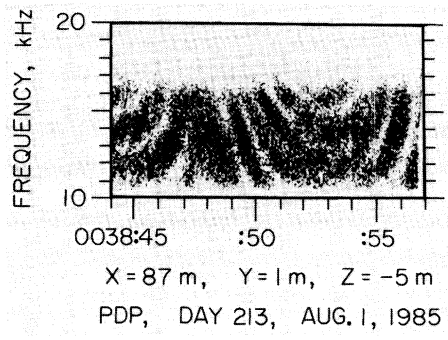


Fig. 2. An example of an interference pattern observed in the 10- to 20-kHz electric field wideband spectrum. This frequency-time spectrum was obtained over a 13-s interval (0038:42 to 0038:55 UT) on August 1, 1985. The quantities $X$, $Y$, and $Z$ are local vertical/local horizontal (LVLH) coordinates.

the ionospheric plasma rest frame near the lower hybrid frequency and wave vector directions almost perpendicular to the magnetic field. Type 1 interference patterns have been studied in detail by *Feng et al.* [1992]. These interference patterns resulted from oblique ion acousticlike waves driven by a return current associated with the ejected electron beam. This paper concentrates on type 2 interference patterns, which are associated with lower hybrid waves. A brief theoretical review of interference patterns is given in section 2. The observations are presented in section 3. The observational results are analyzed and the characteristics of the observed lower hybrid waves are given in section 4. A special type of interference pattern called a "tilted" interference pattern is discussed in section 5. In section 6 the effect of thruster firings on the occurrence of the lower hybrid waves is discussed. A comparison with previous theoretical work [*Cairns and Gurnett*, 1991*a*, *b*; *Rivas and Hastings*, 1992] is given in section 7. Finally, the conclusions are given in section 8.

## 2. Interference Patterns

"Fingerprint" patterns in frequency-time spectrograms are a well-known space plasma wave phenomena. They are caused by electrostatic waves with different wavelengths that are short compared to the antenna length [*Temerin*, 1979; *Fuselier and Gurnett*, 1984; *Gallagher*, 1985; *Feng et al.*, 1992]. Typically, a periodic pattern of constructive and destructive interference is produced by the spin-related rotation of the antenna in the wave field. For fingerprint patterns to be observed, two conditions must be met: (1) the Doppler shift of the waves has to be quite large compared to the rest frame wave frequency, and (2) waves with the same wavelength must propagate in almost the same direction. The frequency-time spectrum in the wideband data can then be regarded as the wavenumber (or wavelength)-time spectrum. An example of an interference pattern observed in the PDP data is shown in Figure 2.

The coordinate system used in the analysis of the Spacelab 2 data is the local vertical/local horizontal (LVLH) reference system (Figure 3). The $Z$ axis lies along the geocentric radius vector to the shuttle and is positive toward the center of the Earth. The $X$ axis lies in the orbital plane and is positive in the direction of spacecraft motion. The $Y$ axis completes the right-handed orthogonal system. The space shuttle's center of mass defines the origin of the coordinate system. The PDP electric field antenna consisted of two spherical probes separated by a distance $l$ of 3.89 m. During the free flight mission the antenna rotated in the $X$-$Z$ plane. Except near magnetic conjunctions, the PDP was close to the $X$-$Z$ plane.

*Feng et al.* [1992] have previously studied the type 1 interference patterns observed by the PDP. These are due to oblique ion acousticlike waves associated with the electron beam generated by the fast pulse electron gun experiment [*Reeves et al.*, 1988]. *Feng et al.* [1992] showed how interference patterns could be used to determine the wavelength, the direction of propagation, the Doppler shift, the rest frame frequency, the angular distribution, and the power spectrum of waves as a function of wave number. As shown by *Feng et al.* [1992], the voltage $V_m$ detected by a dipole antenna rotating in an electrostatic wave field is given by

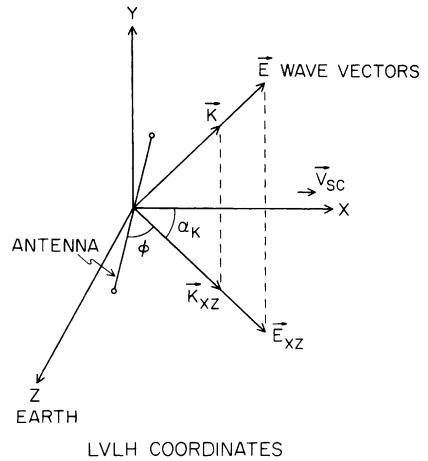


Fig. 3. The orientation of the PDP antenna in the LVLH coordinate system. The $Z$ axis in the LVLH system lies along the geocentric radius vector to the spacecraft and is positive toward the center of the Earth. The $X$ axis lies in the orbital plane and is positive in the direction of spacecraft motion. The $Y$ axis is normal to the orbital plane and completes the right-handed orthogonal system.

$$V_m = \frac{E_{xz} l}{\sqrt{2}} |\cos \phi| \left| \frac{\sin (x \cos \phi)}{x \cos \phi} \right| \quad (1)$$

where

$$x = \frac{k_{xz} l}{2}$$

The quantities $E_{xz}$ and $k_{xz}$ are the magnitudes of the projections of the electric field **E** and wave vector **k** onto the $X$-$Z$ plane and $\phi$ is the angle between the projection $\mathbf{k}_{xz}$ of the wave vector onto the $X$-$Z$ plane, and the antenna axis **l**. In the wideband data, $\mathbf{k}_{xz}$ is related to the measured frequency though the Doppler shift, while $\phi$ varies with time. The wave vector $\mathbf{k}_{xz}$ and angle $\phi$ control the shape of the interference pattern in the frequency-time spectrum. If $\lambda \sim l$, then the $|\sin (x \cos \phi)/x \cos \phi|$ term produces a characteristic spin-modulated interference pattern that can be observed in the wideband spectrums. The minima in the measured voltage occur when $\sin (x \cos \phi)$ is zero. This condition can be expressed as

$$\frac{k_{xz} l \cos \phi}{2} = m \frac{\pi}{2} \quad (2)$$

where $m$ is an even number ($m = 2, 4, 6, \cdots$). Maxima occur when $\tan (x \cos \phi) = (x \cos \phi)$, or approximately where $m = 0, 2.86, 4.92, 6.94, \cdots$. Note that at $m = 0$ the voltage has its largest maximum.

The interference pattern usually has a U-shaped appearance on a frequency-time spectrogram since larger and larger projected wave vectors are required to meet the null condition when the angle $\phi$ approaches $\pm\pi/2$. The angle $\phi$ and the magnitude of the wave vector $\mathbf{k}_{xz}$ projected onto the $X$-$Z$ plane can be determined for each null and maximum position at the center of the U-shaped interference pattern. Using the Doppler shift equation,

$$\omega' = \omega_0 - \mathbf{k} \cdot V_{sc}, \quad (3)$$

the rest frame frequencies $\omega_0$ can then be obtained by subtracting the Doppler shift from the measured frequencies $\omega'$ of the nulls and maximums. Here $V_{sc}$ is the velocity of the shuttle relative to the ambient ionospheric plasma. The dispersion relation of the waves can therefore be determined. Note that the interference pattern analysis gives no information on the component of the wave vector perpendicular to the antenna spin plane ($X$-$Z$ plane). Fortunately, for the PDP data the perpendicular component of the wave vector does not enter into the Doppler shift calculation since $V_{scy} = 0$. The rest frame power spectrum and the angular distribution of the waves can be also deduced from the wideband interference patterns. From *Feng et al.* [1992] the measured spectral density is given by

$$P_{\text{mea}}(\mathbf{k}_{xz}, \phi) = \left(\frac{V_m^2}{\Delta f}\right)_{\text{mea}} = \frac{E_0^2(\mathbf{k}_{xz})}{2\Delta f} l^2 \cdot \int F(\alpha_k) \frac{\sin^2 \{x(\alpha_k) \cos [\phi(\alpha_k)]\}}{x^2(\alpha_k)} d\alpha_k \quad (4)$$

where $E_0(\mathbf{k}_{xz})$ is the true electric field and $\Delta f$ is the measurement bandwidth. The function $F(\alpha_k)$ gives the distribution of wave vectors at propagation angle $\alpha_k$. In section 4, (4) is used to numerically simulate interference patterns and to estimate the true electric field density spectrum as a function of wave number $k_{xz}$ (or frequency) from the wideband interference pattern [cf. *Feng et al.*, 1992].

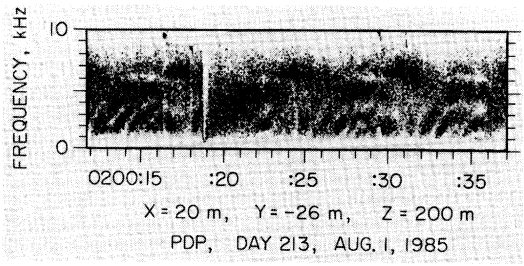


Fig. 4. An example of an interference pattern observed in the 0- to 10-kHz electric field wideband spectrum. This spectrum was obtained over a 25-s interval (0200:12 to 0200:37 UT) on August 1, 1985. The quantities $X$, $Y$, and $Z$ are LVLH coordinates.

## 3. OBSERVATIONS

The PDP wideband receiver provides measurements in both the ELF (0–1 kHz) range and the VLF (0.4–30 kHz) range. The interference patterns of interest for this study were observed in the VLF frequency range. During the PDP free flight the wideband receiver was connected alternately to the 3.89-m double-sphere electric antenna and to the 16-inch 10,000-turn search coil magnetic antenna. Every fourth magnetic antenna period was replaced by a Langmuir probe period. The VLF bands were subjected to an additional switching pattern. In each 52.8-s antenna period (cycle), the frequency range 0.4 to 10 kHz was measured first for 25.6 s, then the 20- to 10-kHz range (with inverted frequency response) was measured for 12.8 s and then the 20- to 30-kHz range was measured for 12.8 s. The antenna switching pattern and the frequency band switching pattern account for the apparent gaps and discontinuities in the wideband data as well as a lack of simultaneous electric and magnetic field wideband observations. The analog wideband output signal was kept within closely controlled limits by an automatic gain control (AGC). Because of the AGC, the absolute intensity of the waves cannot be obtained directly from the wideband data.

During the 6-hour free flight mission, type 2 interference patterns were observed more than 20 times in the 0- to 10-kHz and 10- to 20-kHz electric field wideband data. These interference patterns have different characteristics in the two frequency bands. In the 10- to 20-kHz frequency band the U-shaped interference pattern always opens upward. An example of this type of interference pattern is shown in Figure 2. In the 0- to 10-kHz frequency band, the U-shaped interference pattern always opens downward. An example of this type of interference pattern is shown in Figure 4. The interference patterns are symmetric about the lower hybrid frequency, which is typically 6 ~ 9 kHz. The lower hybrid frequency $\omega_{\text{LHR}}$ can be obtained from

$$\frac{1}{\omega_{\text{LHR}}^2} = \frac{1}{\Omega_{ce}\Omega_{ci}} + \frac{1}{\omega_{pi}^2} = \frac{m_{O+}}{m_e}\left(\frac{1}{\Omega_{ce}^2} + \frac{1}{\omega_{pe}^2}\right) \quad (5)$$

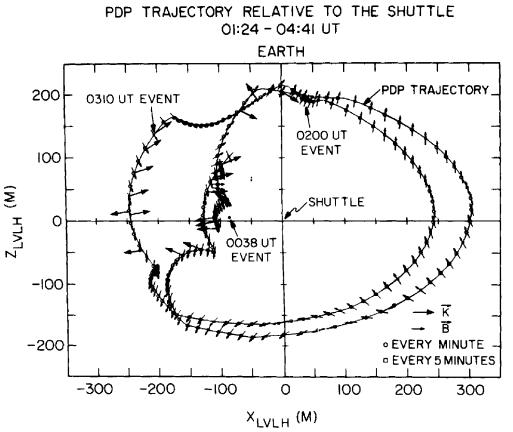


Fig. 5. The wave vector directions and magnetic field directions plotted as a function of the $X$, $Z$ position of the PDP during the period from 0124 to 0441 UT.

where $\omega_{ce}$ is the electron cyclotron frequency, $\omega_{ci}$ is the oxygen ion cyclotron frequency, $\omega_{pe}$ is the plasma frequency, and $\Omega_{pi}$ is the oxygen ion plasma frequency. For the Spacelab 2 environment, $\omega_{pe}$ is $\sim 3\Omega_{ce}$. Therefore the second term on the right side of (5) is a minor term. In this case, (5) can be simplified to

$$\omega_{\mathrm{LHR}} \approx (m_e/m_{\mathrm{O}+})^{1/2}\, \Omega_{ce}.$$

The lower hybrid frequency can then be computed directly from the magnetic field, which was measured by a magnetometer on the PDP. For the events in Figures 2 and 4 the lower hybrid frequency is 8.2 and 6.5 kHz, respectively. The interference patterns in the 0 to 10 kHz band will be shown in this paper correspond to lower hybrid waves that are Doppler-shifted to lower frequencies (i.e., propagating upstream), while the interference patterns in the 10- to 20-kHz band correspond to lower hybrid waves that are Doppler-shifted to higher frequencies (i.e., propagating downstream).

The wave vector direction in the $X$-$Z$ plane can be determined from the center of the U-shaped interference pattern and the direction (up or down) of the U-shape. In Figure 5 the wave vector and magnetic field directions for the lower hybrid-wave interference patterns are plotted along the PDP trajectory in the $X$-$Z$ plane. The magnetic field direction is shown with a short arrow while the wave vector direction is shown with a long arrow. Wave vectors pointing downstream correspond to interference patterns observed in the 10–20 kHz band, and wave vectors pointing upstream correspond to interference patterns observed in the 0–10 kHz band. The plotted events all occur between 0124 and 0441 UT. Several similar interference patterns occurred either before or after this time period. However, since the PDP remained ~90 m directly downstream from the shuttle and moved little with respect to the shuttle during this period, these wave vector directions are not shown in Figure 5. They all have similar characteristics to those shown in Figure 5. All of these events were measured downstream from magnetic field lines connected to the shuttle. This relationship suggests that the waves are produced by an interaction that takes place along magnetic field lines linked to the shuttle. As can be seen from Figure 5, the wave vectors are in all cases almost perpendicular to the magnetic field (in the $X$-$Z$ plane). For most of the cases the measured angles with respect to the magnetic field are within the range 80°–90°, with a ±5° error. Large wave normal angles, near 90°, are an identifying characteristic of lower hybrid waves. As we will show in the next section, the rest frame wave frequencies deduced from the interference patterns are in all cases very close to the lower hybrid frequency. From now on we refer to these interference patterns as lower hybrid-type interference patterns.

Comparing Figure 5 with Figure 2 of *Gurnett et al.* [1988], which showed the strong noise region observed by the PDP broadband receiver, we find that the lower hybrid-type interference patterns are strongly associated with high plasma wave intensities. Most of the interference patterns are observed in the regions (dark dots in Figure 2 from *Gurnett et al.* [1988]) where the broadband shuttle-induced wave field exceeds 1 mV/m. Measured power spectra at 0310 and 0450 UT are shown in Figure 6. These spectra were obtained from the Helios and MFR spectrum analyzers which provide 24 channels covering the frequency range from a 31 Hz to 17.8 MHz. The wave activity is clearly enhanced near the lower hybrid frequency. The wave activity reaches the highest level around lower hybrid resonance in the 0450 UT event and the second highest level during the 0310 UT event. The locations of the lower hybrid-type interference patterns can be divided into two groups. The first group, which includes most events, was observed in the shuttle wake region when the PDP was ~100 meters downstream from the shuttle (0030 to 0130 UT and 0350 to 0455 UT), and ~250 meters directly downstream from the shuttle (0255 to 0312 UT). The second group, which includes the 0200 UT event (see Figure 4), was observed when the PDP was approaching magnetic conjunction from the downstream direction (i.e., in the region directly downstream of the magnetic field lines through the shuttle). Both upward and downward Doppler shifts (corresponding to downstream and upstream propagation) were observed in each group of events.

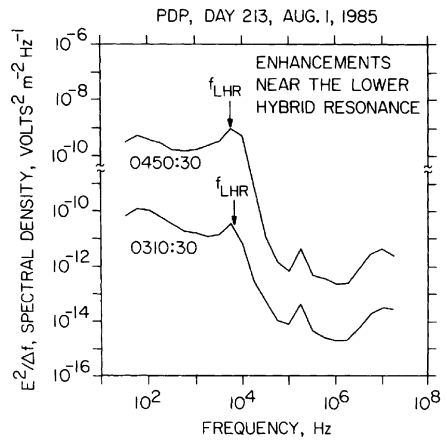


Fig. 6. The electric field spectral density as a function of frequency during the 0310 and 0450 UT events. Clear enhancements are evident near the lower hybrid resonance.

An interesting new phenomenon observed in association with the lower hybrid waves is the occurrence of asymmetric or "tilted" interference patterns, for example, the 0310 UT event in Figure 7. This event is from a series of lower hybrid-type interference patterns that was observed from 0250 to 0310 UT when the PDP was completing the last wake crossing well downstream from the shuttle. However, only the last one near 0310 UT was clearly asymmetric. This event occurred just after the PDP had crossed the wake region. The position of the PDP along the $Z$ axis had increased to ~140 m in the shuttle rest frame. "Tilted" interference patterns were also observed at 0150, 0200, and 0325 UT. The tilted interference patterns all occurred when the PDP had a relatively large $Z$ position in the shuttle rest frame. Considering that the magnetic field is usually oriented somewhat out of the $X$-$Z$ plane (20° to 30°), the PDP was not directly downstream from the shuttle at these times. The interpretation of these asymmetric interference patterns will be discussed in detail in the section 5.

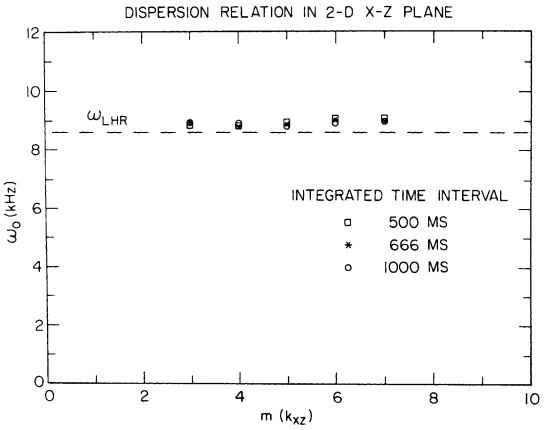


Fig. 8. The dispersion relation of the lower hybrid waves in the two-dimensional $X$-$Z$ plane for the 0038 UT event.

## 4. Analysis of the Interference Patterns

As has been previously discussed, the angle between the wavevector and the ambient ionospheric plasma flow direction ($X$ axis) can be determined from the center of U-shaped interference patterns. The magnitude of the wave vector projected onto the $X$-$Z$ plane $\mathbf{k}_{xz}$ can also be determined from (2) for each maximum and null. The motion of the PDP relative to the shuttle (~1 m/s) is much less than the shuttle speed (7.4 km/s) and can be neglected when calculating the Doppler shift. By subtracting the Doppler shift term, $k_{xz}V_{sc}\cos\alpha$ from the measured wave frequency, the wave frequency in the ambient ionospheric rest frame can be computed using (3) for each maximum and null. The corresponding wavenumbers and frequencies give the dispersion relation of the wave. The dispersion relation for the waves near 0038 UT is shown in Figure 8. The rest frame wave frequencies are very close to and a little above the lower hybrid frequency $\omega_{LHR}$. The dispersion relation has also been computed for the 0128 and 0200 UT events where interference patterns are clearly present. They have characteristics similar to those shown in Figure 8. The other interference patterns are not clear enough to determine a reliable dispersion relation. Usually only one or two nulls or maximums can be determined. Nevertheless, the rest frame frequency can still be computed from the nulls and maximums. For ten interference patterns that were measured, it is found that the wave frequency is always very close to the lower hybrid frequency in the plasma rest frame.

The relative power as a function of wave number (or wavelength) can also be determined for each interference pattern using the technique of *Feng et al.* [1992]. The resulting spectrum only covers the wideband frequency region (0.4 to 20 kHz) and includes only relative intensities because the AGC eliminates absolute intensity information. The true power spectrum $E_0^2(k_{xz})$ is computed from the measured power spectrum using (4) to eliminate interference effects. The degree of clarity of the interference pattern depends on the angular distribution of wave vectors $F(\alpha_k)$ (for the same wave number). A Gaussian distribution is assumed for the wave angular distribution $F(\alpha_k)$ when we deduce the true power spectrum. The variable standard deviation is minimized in order to find the best fit to the angular distribution. Therefore both the power spectrum and the angular distribution of the waves $F(\alpha_k)$ can be determined from the best fit. Figure 9 shows the best fit power

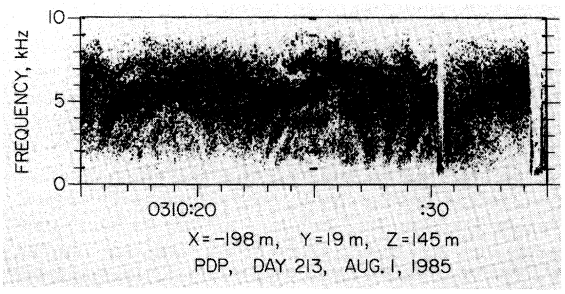


Fig. 7. A tilted interference pattern observed in the 0- to 10-kHz electric field wideband spectrum. This spectrum was obtained over a 20-s interval (0310:15 to 0310:30 UT) on August 1, 1985.

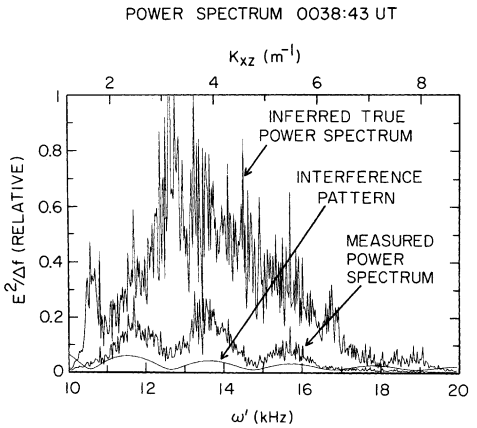


Fig. 9. Inferred true power density spectrum obtained from the measured power density spectrum by eliminating the antenna interference effect for the 0038 UT event.

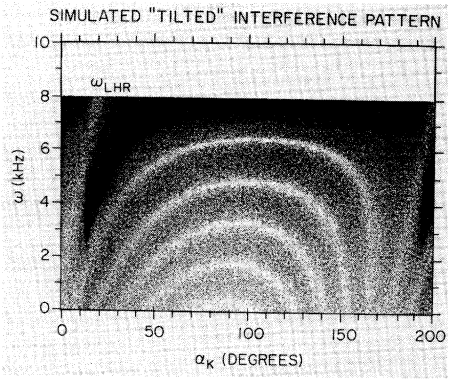


Fig. 10. A computer-generated simulation of a tilted interference pattern.

spectrum for the 0038 UT event. The best fit is obtained when the standard deviation in $\alpha_k$ is assumed to be ~5°. The range of wavelengths for the lower hybrid waves is 1 ~ 4 m, with the intensity peaking near 2 m.

## 5. Tilted Interference Patterns

Most of the lower hybrid interference patterns have a vertical symmetry axis through the center of the U shape. This type of symmetry occurs whenever waves with different wavelengths have the same wave vector direction. However, as shown in Figure 7, in some cases asymmetric, tilted interference patterns were observed by the PDP. Asymmetric interference patterns may have been presented but have never been discussed, in previous papers [*Temerin*, 1979; *Fuselier and Gurnett*, 1984; *Gallagher*, 1985]. Basically, the distortion of the interference pattern could be caused by either time variations in the wave vector or by multiple wave sources. The time variations could be caused by the PDP moving relative to the shuttle, or by a change in the ambient plasma conditions such as the magnetic field direction. A relative change (with time) in the wave vector direction will cause phase changes which could make the interference pattern asymmetric. However, the phase should change the same amount for all wave numbers. Such time-varying phase changes cannot explain the observed tilted interference patterns because of the following:

1. The tilted interference patterns have been observed repeatedly for several continuous antenna spin periods. The time interval between two interference patterns is consistent with the antenna spin periods (13.6 s). This suggests that phase changes are not responsible for the tilted interference patterns. A phase change would enlarge or shorten the time interval between two interference patterns.

2. The asymmetric interference patterns caused by phase changes should be compressed on one side, but the center of the various nulls and maxima should remain at the same phase. Such distortion makes the interference pattern asymmetric, but not tilted in the manner observed by the PDP.

We believe the tilted interference patterns observed by the PDP are not caused by time variations but by the following idea: tilted interference patterns occur whenever waves with different wavelengths have wave vector distributions centered at different propagation directions in the $X$-$Z$ plane. In this case the angle $\alpha_{k0}$ becomes a function of wave number $k_{xz}$. Different nulls and maxima are then centered at different times or angles $\phi$, which makes the U-shaped pattern tilt. A simulation of a tilted interference pattern is shown in Figure 10. This pattern is based on (4) with a constant electric field $E_0(k_{xz})$ and an angle $\alpha_{k0}$ that varies linearly with the wave number $k_{xz}$. The rest frame frequencies are assumed to be constant at the lower hybrid frequency (8 kHz) with a downward Doppler shift in the shuttle rest frame. A Gaussian distribution with a 5° standard deviation in $\alpha_k$ is assumed for $F(\alpha_k)$ in (4). The overall change in angle $\alpha_{k0}$ is $<15°$ for the range of observable wave numbers in Figure 10. As can be seen, even for this simple linear model, the calculated shape agrees very well with the observed shape.

The variation in the wave vector and group velocity direction as a function of wave number is the fundamental reason that tilted interference patterns can occur. However, geometry, propagation effects, and multiple wave sources almost certainly play a role in forming the tilted interference patterns. The wave vectors of the lower hybrid waves are directed almost perpendicular to the magnetic field, differing by only 1°–2° under Spacelab 2 conditions according to linear theory. If the waves propagate close to the $X$-$Z$ plane and are perpendicular to the magnetic field which lies within 30° of the $X$-$Z$ plane during the Spacelab 2 mission, the wave vectors projected onto the $X$-$Z$ plane would point in almost the same direction for all wave numbers. Therefore one can argue that waves propagating primarily in the $X$-$Z$ plane cannot form tilted interference patterns. The component of the wave vector $\mathbf{k}_y$ has to be quite large for a tilted interference pattern to occur. For lower hybrid waves the group velocity varies with the wave number. Waves with different wavelengths are therefore likely to come from different source regions. When the wave vectors are projected onto the $X$-$Z$ plane, waves that reach a given location from different source regions propagate in different directions. The direction may vary a significant amount if $k_y$ is large enough. This general explanation is consistent with the observations since all the tilted interference patterns were observed when the PDP had a relatively large $Z$ position in the shuttle rest frame (i.e., when the PDP was not directly downstream from magnetic field lines connected to the shuttle). During these events the PDP is not directly downstream from the water cloud around the shuttle, which is the likely source of the ions responsible for generating the lower hybrid waves [*Cairns and Gurnett*, 1991*a*, *b*]. For the 0310 UT event (Figure 7) the magnetic field was ~30° out of the $X$-$Z$ plane. As shown in Figure 11 in the $Y$-$Z$ plane, the PDP was ~55 m away from the point magnetically conjugate with the shuttle. Assuming that the waves were generated near the magnetic field line through the shuttle, this geometry suggests that the waves propagated ~60 m in the ambient plasma rest frame and convected ~130 m along the $X$ axis. For this geometry the group speed of the waves would be approximately half the shuttle speed relative to the ambient ionospheric plasma $V_{sc}$, which is ~10 times the ion thermal speed. Such high group speeds are not consistent with the observed dispersion relation from Figure 8. Therefore the source region was probably not near the shuttle but more likely some point along the $X$ axis through the PDP and relatively far from the shuttle (>40 m).

## 6. LOWER HYBRID WAVES ASSOCIATED WITH THRUSTER FIRINGS

The shuttle thrusters were fired frequently during the PDP free flight period. The thrusters caused the yellow spikes at extremely low frequencies on the color-coded spectrums in Plates 1 and 2 of *Cairns and Gurnett* [1991*a*]. These spikes can also be seen in the wideband data, for instance at 0200:19 UT in Figure 4. From a model of the thruster plume [*Hoffman and Hetreck*, 1982] it is estimated that the density of neutral gas produced from the thruster 100 m away from the shuttle is approximately $10^{12}$ cm$^{-3}$, which is a 1000 times higher than the ambient plasma density. The correlation between the amplitude of the electrostatic waves and thruster firings has been studied by *Gurnett et al.* [1988]. Although most of the lower hybrid waves are not directly related to thruster firings, many of the lower hybrid-type interference patterns were observed during times of high thruster activity. We also found some cases in which thruster firings were directly responsible for the observed lower hybrid waves, for example near 0323 and 0326 UT as shown in Figure 12. Figure 12 is the gray-coded broadband electric field spectrums with Helios and MFR data for the time periods 0319–0328 UT. In the low-frequency range, beside the regular antenna spin modulation, the thruster caused the darker spikes extended above the lower hybrid frequency. During these periods the PDP was approaching a magnetic conjunction with the shuttle. The background electric field levels are relatively low. Right after each thruster firing, which typically has a duration of less than a second, the lower hybrid waves were enhanced for 20 ~ 30 s. Since the neutral gas released from thruster firings has a much higher density than the ambient atmosphere around the shuttle, it is clear that thruster firings should enrich the shuttle water cloud for a considerable period of time, thereby enhancing the level of lower hybrid waves driven by pickup ions. In general, both water vapor leaking from the shuttle and neutral gas produced by the thruster firing apparently contribute to the neutral water cloud surrounding the shuttle. This coupling of the thruster material and the atmosphere around the shuttle should be further investigated.

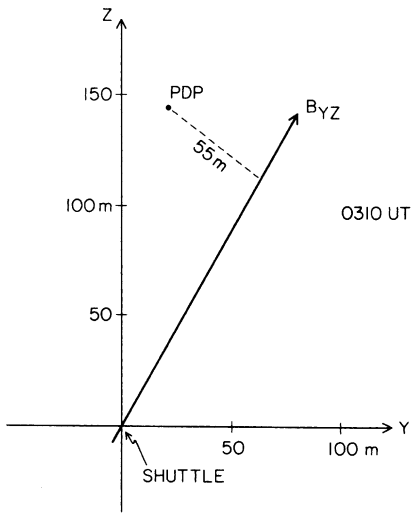


Fig. 11. The position of the PDP relation to the magnetic field connecting to the shuttle for 0310 UT event.

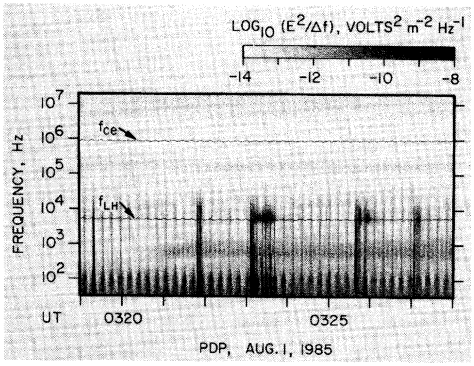


Fig. 12. A broadband electric field spectrogram with Helios and MFR data for the time periods 0319–0328 UT. The electric field spectral density is gray-coded with white being the least intense and black being the most intense. The white curves labeled $f_{ce}$ and $f_{LH}$ are the electron cyclotron and lower hybrid frequencies, respectively.

## 7. COMPARISON WITH PREVIOUS THEORETICAL WORK

The lower hybrid waves observed around the shuttle are almost certainly generated by an interaction between the ambient ionospheric plasma and the neutral water cloud surrounding the shuttle [*Gurnett et al.*, 1988; *Paterson and Frank*, 1989; *Cairns and Gurnett*, 1991*a*, *b*]. As described above, there are two major sources contributing to the neutral water cloud. One is the steady outgassing of water molecules from the shuttle, and the other is the shuttle thrusters. *Cairns and Gurnett* [1991*a*] pointed out that the amplitude and spectral character of the low-frequency electrostatic waves observed during the PDP free flight was controlled by the angle between the magnetic field and the shuttle velocity relative to the ionospheric plasma. When the shuttle velocity is approximately perpendicular to the magnetic field, large wave amplitudes and the characteristic mushroom-shaped frequency-time structures are observed in the broadband spectrum (see the semilog scale plot in Figure 1), whereas more nearly parallel flows are characterized by low wave levels. The top line of the mushroom is near the lower hybrid frequency. The base of the mushroom is a triangular-shaped emission that starts at low frequencies and extends up to the lower hybrid frequency near the center of the mushroom. For the observed broadband spectrum, see Plates 1 and 2 of *Cairns and Gurnett* [1991*a*]. The correlation between the spectral features of the mushroom and the magnetic field angle has a natural interpretation in terms of the optimum conditions for wave growth driven by pickup ions and the time available for evolution of the wave spectrum [*Cairns and Gurnett*, 1991*a*]. The pickup ions are produced from the outgassing water molecules though collisional charge exchange processes with ionospheric $O^+$ ions [*Paterson and Frank*, 1989; *Cairns*, 1990]. When the shuttle velocity has a significant component along the magnetic field, the pickup ions have gyrocenter velocities in a different plane from the ambient plasma and rapidly separate from the wave region downstream from the shuttle. The pickup ions

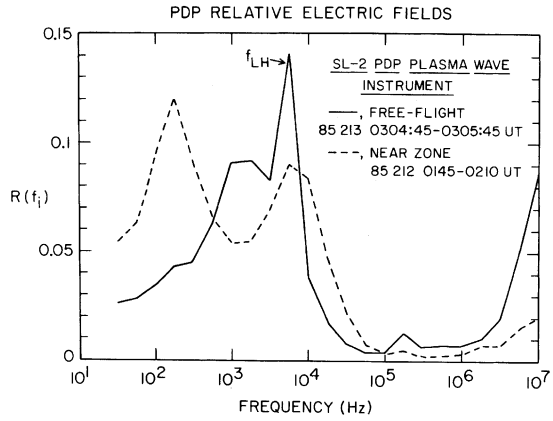


Fig. 13. Comparison of the relative electric field spectra for the near zone and the free-flight waves. The dashed line is the averaged spectra for the near zone waves during the interval 0145 to 0210 UT on day 212, 1985. The solid line is the free-flight spectra measured at the center of the mushroom during the interval 0304:45 to 0305:45 UT on day 213, 1985.

will then have little time to interact with the ambient ionospheric plasma and produce wave growth. On the other hand, if the shuttle velocity vector is perpendicular to the magnetic field then the pickup ions remain in the wave region for a long time, leading to the growth of large amplitude waves.

*Cairns and Gurnett* [1991*b*] studied the characteristics of the near zone waves observed within 10 m of the shuttle during the Spacelab 2 mission. At that time the PDP was attached to the rms arm and remained in the same position (~10 m away) relative to the shuttle. As shown by the dashed curve in Figure 13, the relative electric field spectrum of the near zone waves (averaged over a 25-min interval from 0145 to 0210 UT on day 212, 1985) has three components: one peak near the lower hybrid frequency, another peak at lower frequencies (~200 Hz), and a relatively continuous uniform component between the two peaks [*Cairns and Gurnett*, 1991*b*]. The solid line shown in Figure 13 gives the relative electric field spectrum measured over a 1-min interval (0304:45 to 0305:45 UT, day 213, 1985) at the center of a mushroom during the free flight mission. The average absolute spectral density for both cases is shown in Figure 14. As can be seen, the waves observed in the near zone and the waves observed during the free flight have similar spectra and are within the same intensity range. In the free flight case the relative electric field spectrum also has a peak around the lower hybrid frequency and a similar uniform region, but the peak at lower frequencies is of diminished intensity. The similarities strongly imply that the waves observed at the top and center of the mushroom are generated in the near zone region around the shuttle. The differences between the two spectra at low frequencies imply that the lower frequency waves may be heavily damped, since the lower-frequency peak appeared in the near zone spectrum but not in the free flight spectrum. Thruster firings may also enhance the lower-frequency peak in the near zone case. Note that no thruster firings occur during the free flight period chosen.

*Cairns* [1990] has proposed a model for the water ion distribution surrounding the shuttle based on the observations by *Paterson and Frank* [1989]. He proposed that a distribution of water ions in the form of a beam arc distribution is formed in the vicinity of the shuttle. This distribution, which has both ringlike and beamlike characteristics, varies with distance from the shuttle: it is a ring far from the shuttle and has strong beamlike distribution very close to the shuttle. *Cairns and Gurnett* [1991*a*, *b*] proposed that the waves observed in the mushroom structures and the near zone region are Doppler-shifted lower hybrid waves driven by ring and beam distributions of pickup water ions, respectively. In the shuttle rest frame the beam-driven waves are Doppler shifted downward to a lower-frequency range. Linear theory shows that the beam-driven waves cover the entire frequency range from zero frequency to $\omega_{LHR}$. The wavelengths are 1 to 4 m and within the detectable range of the plasma wave antenna on the PDP. The waves also propagate almost perpendicular to the magnetic field, as expected. Linear theory also shows that the beam distribution has a broader growth region and tends to apply to the uniform region between the two observed near zone peaks. On the other hand, the ring distribution tends to produce waves primarily at lower frequencies, perhaps explaining the low-frequency peak near 200 Hz. These linear analyses assumed that the shuttle velocity is exactly perpendicular to the magnetic field. *Cairns and Gurnett* [1991*b*] suggested that nonlinear and other effects may produce the peak localized near the lower hybrid frequency $\omega_{LHR}$. *Cairns and Gurnett* [1991*a*] also suggested that the waves are produced both very near to the shuttle and throughout the region with pickup ions.

On the basis of the theory of *Cairns and Gurnett* [1991*a*, *b*], *Rivas and Hastings* [1992] have done further work on the near zone waves for a beam arc distribution. Their linear theory uses a series of beamlets to make up a homogeneous beam-arc distribution. The beam-arc is finite and extends over an angle $\Delta\Theta$ in velocity space. For small arcs, $\Delta\Theta < \Delta\Theta_{crit} \approx 60°$, *Rivas and Hastings* [1992] consider the beam-arc plasma instability to be hydrodynamic, while for arcs

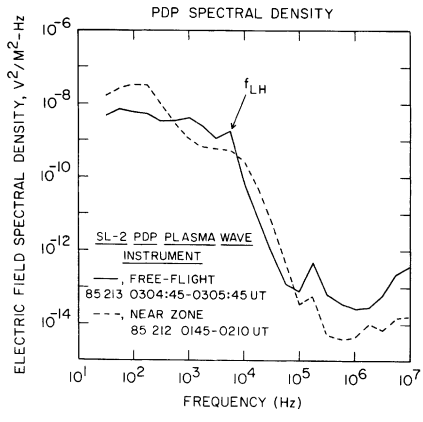


Fig. 14. Comparison of average electric field spectral density as a function of the frequency between the near zone and free-flight waves. The dashed line shows the near zone spectra during the interval 0145 to 0210 UT on day 212, 1985. The solid line is the free-flight spectra measured at the center of the mushroom during the interval 0304:45 to 0305:45 UT on day 213, 1985.

larger than $\Delta\Theta_{crit}$ it is kinetic. Their linear analysis also assumed the shuttle velocity to be exactly perpendicular to the magnetic field which is rarely true during the Spacelab 2 mission. Usually, the magnetic field direction is 20°–30° out of the $X$-$Z$ plane. In order to distinguish the difference between the theory and the true situation, we replace the theoretical $X$-$Z$ plane of *Rivas and Hastings* [1992] with the $X'$-$Z'$ plane. The $X'$ axis is the same as the $X$ axis in the LVLH coordinate system, but the $Z'$ axis is along the magnetic field direction. The waves which propagated out of the $X'$-$Z'$ plane were also investigated. The critical angle $\Delta\Theta_{crit}$ is larger for waves propagating out of the $X'$-$Z'$ plane. For finite beam-arcs this dependence causes waves propagating within the $X'$-$Z'$ plane to be kinetic, while waves propagating out of the $X'$-$Z'$ plane are more likely to be hydrodynamic. These two sets of waves then grow in different wavenumber regions and are Doppler-shifted into different frequency regions. Therefore Rivas and Hastings interpreted the top cap of the mushroom as lower hybrid waves propagating within the $X'$-$Z'$ plane while the base of the mushroom is interpreted in terms of lower hybrid waves propagating out of the $X'$-$Z'$ plane. They also suggested that the major source of the free-flight waves is the convection of waves from the near zone region around the shuttle. This is consistent with the comparisons of near zone and free-flight waves shown in Figure 13 and Figure 14.

The lower hybrid type interference patterns observed in the wideband data correspond to the "uniform" and "lower hybrid" components defined by *Cairns and Gurnett* [1991*b*]. Since the 0–10 kHz wideband channel has a lower cutoff at 400 Hz, no information is available on the low-frequency component observed by *Cairns and Gurnett* [1991*b*] near 200 Hz. As mentioned in the last section, lower hybrid-type interference patterns can be divided into two groups. The first group consists of interference patterns observed directly downstream the shuttle, while the second group consists of interference patterns observed when the PDP is nearly magnetic conjugate with the shuttle. Most of the observed lower hybrid-type interference patterns belong to the first group. The second group includes the tilted interference patterns, which were relatively rare. Since the group speeds of the lower hybrid waves are small compared with the shuttle speed, the waves are mostly convected downstream to the PDP by the ambient ionospheric plasma. The first group is observed almost directly downstream from the shuttle. The source region of these waves should be located in the near vicinity of the space shuttle where the neutral gas density is constantly large. Our observations indicate that the source region is likely to be within 20 m of the shuttle. This implies that convection of the waves generated in the near vicinity of the shuttle is the dominant source of waves observed downstream from the shuttle as suggested by *Cairns and Gurnett* [1991*a*, *b*]. Note that the waves observed near the magnetic conjunctions also correspond primarily to near zone waves with $\mathbf{k} \perp \mathbf{B}$, since the $\mathbf{E}$ fields of these waves vary slowly with distance along magnetic field [*Cairns and Gurnett*, 1991*b*].

As mentioned before, the second group, consisting of tilted interference patterns, is not likely to be generated along magnetic field lines connected to the shuttle and is most likely composed of the waves that are propagating significantly out of the $X$-$Z$ plane. On the other hand, the interference patterns in the first group correspond to near zone waves that mostly propagate within the $X$-$Z$ plane (since they are symmetric interference patterns). The symmetry of the first group of interference patterns is consistent with *Rivas and Hastings*' [1992] interpretation, in which the top cap of the mushroom feature is caused by lower hybrid waves generated in the near zone and propagating mostly within the $X'$-$Z'$ plane. However, the interference patterns cannot provide any information on *Cairns and Gurnett*'s [1991*b*] lower-frequency peak since the lower cutoff of the 0–10 kHz channel is 400 Hz. No interference patterns can be identified in 40–1000 Hz channel, but this channel may be too narrow for interference patterns to be clearly identified. We do have evidence that lower hybrid waves propagate out of $X$-$Z$ plane in the form of tilted interference patterns. However, these waves are not generated in the near zone region of the shuttle. Waves of this type are not considered in the *Rivas and Hastings*' [1992] theory. Therefore we cannot say whether the lower-frequency peak corresponds to lower hybrid waves propagating out of $X'$-$Z'$ plane as proposed by *Rivas and Hastings* [1992].

Another significant difference between the linear theory and the data is the dispersion relation of the waves. The frequencies of the observed lower hybrid waves are very close to and a little above the lower hybrid frequency ($\omega_{LHR}$) in the plasma rest frame and are essentially independent of wavenumber. However, the linear theory [*Cairns and Gurnett*, 1991*a*, *b*; *Rivas and Hastings*, 1992] shows that the waves can be generated over the entire frequency range from 0 to $\omega_{LHR}$ (also in the plasma rest frame) with a primarily beamlike dispersion relation ($\omega_r \sim kV_{sc}$). This difference can be addressed qualitatively in terms of the evolution of the lower hybrid instability: as the instability saturates, the waves may evolve from the beamlike dispersion relation given by the linear theory to the dispersion relation of the lower hybrid mode (in the ambient plasma). This idea is supported by (1) results of *Nishikawa and Cairns* [1991] for electron beam-driven Langmuir waves, and (2) the strong analogy between the ion beam-driven lower hybrid instability and the electron beam instability for Langmuir waves [*Papadopoulos*, 1984; *Cairns and Gurnett*, 1991*b*]. Simulations consistent with these ideas were presented recently by *Rivas et al.* [1992] at the 1992 Fall Meeting of the American Geophysical Union.

## 8. CONCLUSIONS

Antenna interference pattern effects were frequently observed in the PDP plasma wave data during the Spacelab 2 flight. Analysis of these antenna interference patterns permits a determination of the wavelength, the direction of propagation, and the location of the source region. Two types of interference patterns were observed: one type corresponding to waves with very low frequencies (a few hundred hertz) in the plasma rest frame, and the second type corresponding to waves near the lower hybrid frequency. The first type is associated with ion acousticlike waves driven by electron beams ejected from the shuttle. These interference patterns were previously analyzed by *Feng et al.* [1992]. The second type is associated with lower hybrid waves driven by pickup ions from the water vapor cloud around the shuttle and are the subject of this study. Our results show that the lower hybrid waves are generated primarily in the near vicinity of the shuttle. However, tilted

interference patterns suggest that some of these waves are generated well away from the shuttle and the magnetic flux tube threading the shuttle. The wavelength of the lower hybrid waves is relatively short, ~1 to 4 m. The frequencies in the plasma rest frame are very close to the lower hybrid frequency and the waves have an essentially flat dispersion relation that is independent of frequency. The interference pattern analysis confirms *Cairns and Gurnett*'s [1991*a*, *b*] identification of the wave mode and the qualitative details of the instability. The interference patterns correspond to the peak around the lower hybrid frequency and to the uniform component between the two peaks identified in the broadband spectrum by *Cairns and Gurnett* [1991*b*]. The differences between the linear theory and the observational data suggest that the waves evolve into a frequency spectrum with $\omega \sim \omega_{LHR}$. So far, all of the theoretical investigations have been limited to cases in which the magnetic field is exactly perpendicular to the space shuttle velocity, which is rarely true during the PDP free-flight mission. This restriction may severely limit the applicability of the present linear theories since the magnetic field component along the shuttle velocity direction probably plays an important role in both the generation and propagation of the lower hybrid waves. Further work is needed to understand the details of the wave spectrum and the time evolution of the lower hybrid instability, particularly through the use of plasma simulations.

*Acknowledgments.* This research was supported by NASA grants NAGW-1539 and NAGW-2040, and by the University of Iowa Graduate College.

The Editor thanks D. L. Gallagher and D. Hastings for their assistance in evaluating this paper.

## REFERENCES

Cairns, I. H., Transition from ring to beam arc distribution of water ions near the space shuttle orbiter, *J. Geophys. Res.*, *95*, 15,167, 1990.

Cairns, I. H., and D. A. Gurnett, Control of plasma waves associated with the space shuttle by the angle between the orbiter's velocity and the magnetic field, *J. Geophys. Res.*, *96*, 7591, 1991*a*.

Cairns, I. H., and D. A. Gurnett, Plasma waves observed in the near vicinity of the space shuttle, *J. Geophys. Res.*, *96*, 13,913, 1991*b*.

Feng, W., D. A. Gurnett, and I. H. Cairns, Interference patterns in the Spacelab 2 plasma wave data: Oblique electrostatic waves generated by the electron beam, *J. Geophys. Res.*, *97*, 17,005, 1992.

Fuselier, S., and D. A. Gurnett, Short wavelength ion waves upstream of the Earth's bow shock, *J. Geophys. Res.*, *89*, 91, 1984.

Gallagher, D. L., Short-wavelength electrostatic waves in the Earth's magnetosheath, *J. Geophys. Res.*, *90*, 1435, 1985.

Gurnett, D. A., W. S. Kurth, J. T. Steinberg, and S. D. Shawhan, Plasma wave turbulence around the shuttle: Results from the spacelab-2 flight, *Geophys. Res. Lett.*, *15*, 760, 1988.

Hoffman, R. J., and M. A. Hetreck, Jr., Plume contamination effects prediction: Contam III Computer Program, *Tech. Rep. AFRPL TR82-033*, Air Force Rocket Propul. Lab., Edwards Air Force Base, Calif., 1982.

Kurth, W. S., and L. A. Frank, The Spacelab-2 Plasma Diagnostics Package, *J. Spacecr. Rockets*, *27*, 70, 1990.

Nishikawa, K.-I., and I. H. Cairns, Simulation of the nonlinear evolution of electron plasma waves, *J. Geophys. Res.*, *96*, 19,343, 1991.

Papadopoulos, K. D., On the shuttle glow (the plasma alternative), *Radio Sci.*, *19*, 572, 1984.

Paterson, W. R., and L. A. Frank, Hot ion plasmas from the cloud of neutral gases surrounding the space shuttle, *J. Geophys. Res.*, *94*, 3721, 1989.

Pickett, J. S., N. D'Angelo, and W. S. Kurth, Plasma density fluctuations observed during space shuttle orbiter water releases, *J. Geophys. Res.*, *94*, 12,063, 1989.

Reeves, G. D., P. M. Banks, T. Neubert, R. I. Bush, P. R. Williamson, A. C. Frazer-Smith, D. A. Gurnett, and W. J. Raitt, VLF emissions by pulsed and dc electron beam in space, 1, Spacelab 2 observations, *J. Geophys. Res.*, *93*, 14,699, 1988.

Rivas, D. R., and D. E. Hastings, Theoretical interpretation of the electrostatic noise in the space shuttle induced plasma environment, *J. Geophys. Res.*, *97*, 17,097, 1992.

Rivas, D. R., D. E. Hastings, and N. A. Gastonis, Interpretation of the electrostatic waves in the space shuttle induced plasma environment, *Eos Trans. AGU*, *73*, 413, 1992.

Shawhan, S. D., Description of the Plasma Diagnostic Package (PDP) for the OSS-1 shuttle mission and JSC chamber test in conjunction with the fast pulse electron gun (FPEG), in *Artificial Particle Beams in Space Plasma Studies*, edited by B. Grandel, p. 419, Plenum, New York, 1982.

Temerin, M., Doppler shift effects on double-probe measured electric field power spectra, *J. Geophys. Res.*, *84*, 5929, 1979.

I. H. Cairns, W. Feng, and D. A. Gurnett, Department of Physics and Astronomy, University of Iowa, Iowa City, IA 52242.

(Received December 21, 1992;
revised April 30, 1993;
accepted June 16, 1993.)